Diagnostic Studies of a Pinch Plasma Accelerator

DONALD P. DUCLOS,* LEONARD ARONOWITZ,*
FREDERIC P. FESSENDEN,† AND PETER B. CARSTENSEN‡
Republic Aviation Corporation, Farmingdale, N. Y.

Characteristics of a pinch plasma accelerator were investigated by measuring the total discharge current, capacitor voltage, magnetic field distribution, and light front velocity. The current distribution and $J \times B$ force on the plasma were calculated. The results show that a current sheet resulting from the first half-cycle of current propagates along the electrodes, becoming more diffuse with time. It was observed that there are regions in the sheet where the direction of current density shows local reversals. Magnetic probes indicate that the motion of the current sheet turns from an initially radial direction to an axial direction and that the magnetic force on the current sheet is essentially in the direction of plasma motion. The impulse produced by $J \times B$ forces in the accelerator was computed and was found to be the principal contribution to the thrust. All of the net energy output of the capacitor bank was transferred to the accelerator in the first 2.4 μsec.

Introduction

THE pinch plasma accelerator used for this study is shown schematically in Fig. 1. The discharge takes place between a pair of aluminum electrodes of approximately quarter-circle cross section. The inside diameter of the insulator is 8 in. The current is initially concentrated in the region of minimum inductance near the insulator where the electrodes have essentially a linear pinch geometry. The geometry at the exit is that of a coaxial plasma gun. In order that probes could be inserted between the electrodes, holes were drilled through the outer electrode at positions 1–4 shown in Fig. 2. The distances between probes were measured along the centerline of the gap between the electrodes. Unless otherwise noted, the accelerator used a capacitor bank of 12 10-μf capacitors, arranged symmetrically about the electrodes, which were charged to a potential of 3 kv, giving an energy per discharge of 540 joules. The discharge was initiated by briefly opening a solenoid valve that admitted a pulse of gas into the interelectrode space through a set of orifices located in the inner electrode between positions 1 and 2. The propellant used was nitrogen unless otherwise specified. The accelerator was operated in a vacuum chamber held at a pressure of less than 5×10^{-4} mm Hg. Initial diagnostic measurements were reported in Ref. 1.

Figure 3 shows the time variation of the voltage measured at the capacitor terminals and the total discharge current. The voltage was measured with a Tektronix type P6013 voltage divider and the total current with a Rogowski coil and a simple r.c. integrating circuit. It is seen that the greatest portion of the voltage drop occurs during the first microsecond. The half-cycle period of the current is slightly over 3 μsec.

Presented at the AIAA Electric Propulsion Conference, Colorado Springs, Colo., March 11–13, 1963; revision received July 17, 1963. This work was supported in part by the Air Force Office of Scientific Research under Contract AF 49(638)-552. The authors would like to thank W. McIlroy for many stimulating discussions, F. Petri for aiding in the reduction of the experimental data, and the personnel of the experimental laboratory for building and assisting in the operation of the apparatus.

* Specialist Scientific Research Engineer, Power Conversion Systems Division. Member AIAA.

† Senior Scientific Research Engineer, Power Conversion Systems Division.

‡ Scientific Research Engineer, Power Conversion Systems Division. Member AIAA.

It is assumed in linear pinch theory (e.g., see Ref. 2) that the discharge current will begin to flow at the outer periphery of the electrodes. The current produces an azimuthal magnetic field that increases from zero at the leading edge of the current sheet to its maximum value at the trailing edge. The resulting magnetic pressure accelerates the current sheet in the radial direction. As the current sheet moves inward, the magnetic pressure acts as a "piston" that picks up the gas ahead of it. For purposes of calculation, the current sheet is usually assumed to be infinitely thin and the plasma in the sheet to have an infinite electrical conductivity. Also, the magnetic piston is sometimes assumed to pick up and accelerate all of the gas ahead of it (snowplow model) or to accelerate a fixed amount of gas (slug model). In the pinch plasma accelerator, the curved electrodes allow the plasma to turn in the axial direction so that it can be ejected from the accelerator.

One of the purposes of this study was to determine how closely the characteristics of the accelerator resemble the idealized model. In particular, it was desired to determine if the motion of the current sheet turns from the radial to the axial direction and if the magnetic force or "piston" constitutes the primary means of accelerating the plasma, or if the plasma is accelerated by some other means.

Magnetic Field Measurements

In order to study the current sheet, the magnetic field was measured by means of magnetic probes. The probes were constructed of Teflon-covered no. 28 magnet wire wound into an eight-turn solenoid approximately 3 mm in diameter and 3 mm long. The cable from the probe was terminated[3] to provide a flat frequency response up to 8 Mc. The probes were used with simple r.c. integrating circuits with a 47-μsec time constant. Although the probes were in direct contact with the plasma, the Teflon coating provided a satisfactory operating life. It was found that the operating life of the probes could be extended by covering the Teflon-coated wire with a thin coating of epoxy resin. Earlier attempts were made to construct probes that would withstand the plasma environment by enclosing them with quartz covers about 7 mm in diameter and 8 mm long. However, the covers lowered the output signal appreciably and thus were abandoned.

The azimuthal magnetic field B_θ at a given probe position is proportional to the current between the probe and the leading edge of the current distribution. Current between the insulator and the probe does not contribute to the probe

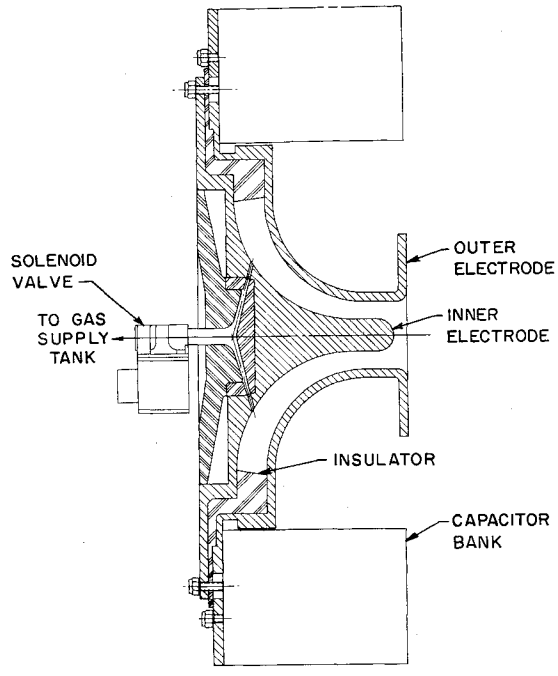

Fig. 1 Schematic of pinch plasma accelerator.

signal. Reproductions of typical oscilloscope traces of B at the four probe positions are shown in Fig. 4. It is seen that the time of arrival of the magnetic field at a given position is later than at the previous position, indicating that the magnetic field does propagate down the electrodes. Since position 1 is near the insulator, the probe signal at this position has an approximately damped sinusoidal form corresponding to the total discharge current. However, it is seen from Fig. 4 that at positions 2–4 the magnetic field always remains positive or has, at most, a slight negative dip. This demonstrates that the current distribution resulting from the second half-cycle does not propagate down the electrodes but remains between the insulator and position 2. This phenomenon is similar to the "self-crowbarring" discussed by Gooding, Hayworth, and Lovberg.[4] However, they observed a second breakdown that occurred before the second half-cycle of current.

The foregoing results contrast with those of Jahn and von Jaskowsky,[5] who studied linear pinch discharges triggered by an external switch. They found that the magnetic field due to the second and succeeding half-cycles did propagate toward the axis. This dissimilarity of results could be associated with the greater external inductance of their apparatus or with differences in gas density.

Times of arrival were also measured at positions 1–4 with a photocell and a single electric probe grounded through a 5-ohm resistor.[1] Comparison of the times of arrival showed that the magnetic probe signal arrived first, followed by the

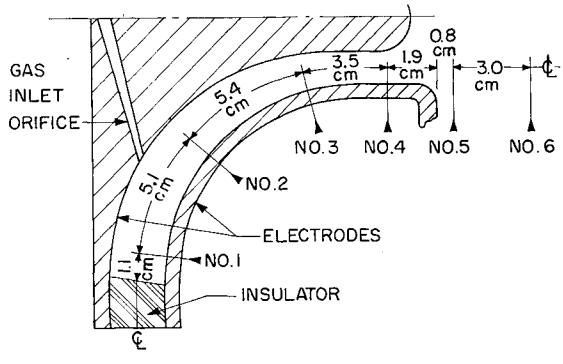

Fig. 2 Accelerator electrodes showing probe positions.

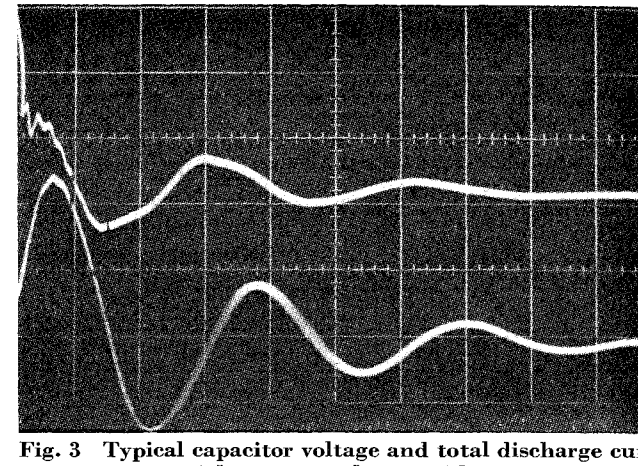

Fig. 3 Typical capacitor voltage and total discharge current traces; initial capactor voltage = 3 kv, sweep speed = 2 μsec/div. Upper trace: V_c, gain = 1 kv/div (zero voltage is three divisions from top). Lower trace: I, gain = 78.4 ka/div.

electric probe signal, followed by the photocell signal. The time of arrival of the magnetic probe signals was about 0.4μsec earlier than the photocell signal. The electric probe signals were roughly midway between the magnetic probe and photocell signals, being somewhat closer to the photocell time of arrival. The delay of the photocell signal could possibly be due to the relaxation times for light emission. The delay of the electric probe signal indicates that there is some current diffusion ahead of the main body of the plasma being accelerated. The electric probes showed a small precursor signal preceding the magnetic probe signal which could be associated with this diffusion. The precursor may be due to photoionization from the main current sheet.

It is seen from Fig. 4 that the oscilloscope traces sometimes show a small positive or negative precursor magnetic field beginning at about $t = 0$. However, the magnitude and time of arrival of the main signal was not affected by the precursor. The precursors may be due to small asymmetries in the current distribution, possibly of the "spoke" type.[4] The current distribution in the discharge, however, is essentially symmetric. This was shown in symmetry tests in which four magnetic probes were located at 90° intervals about the axis of symmetry of the electrodes at the same distance from the insulator. A set of four probes was located at each of the four probe positions shown in Fig. 2. Comparison of the magnitude and time of arrival of the B_θ

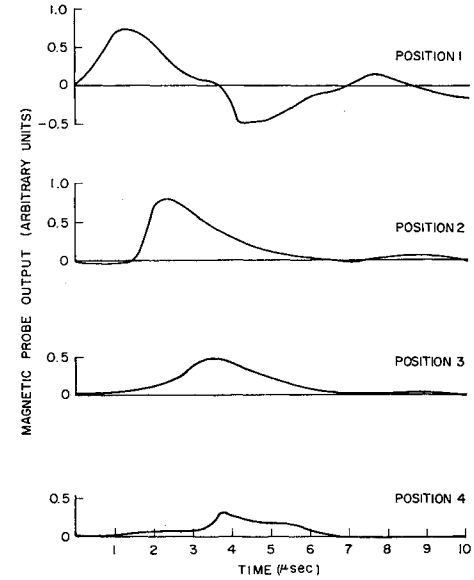

Fig. 4 Magnetic probe output vs time.

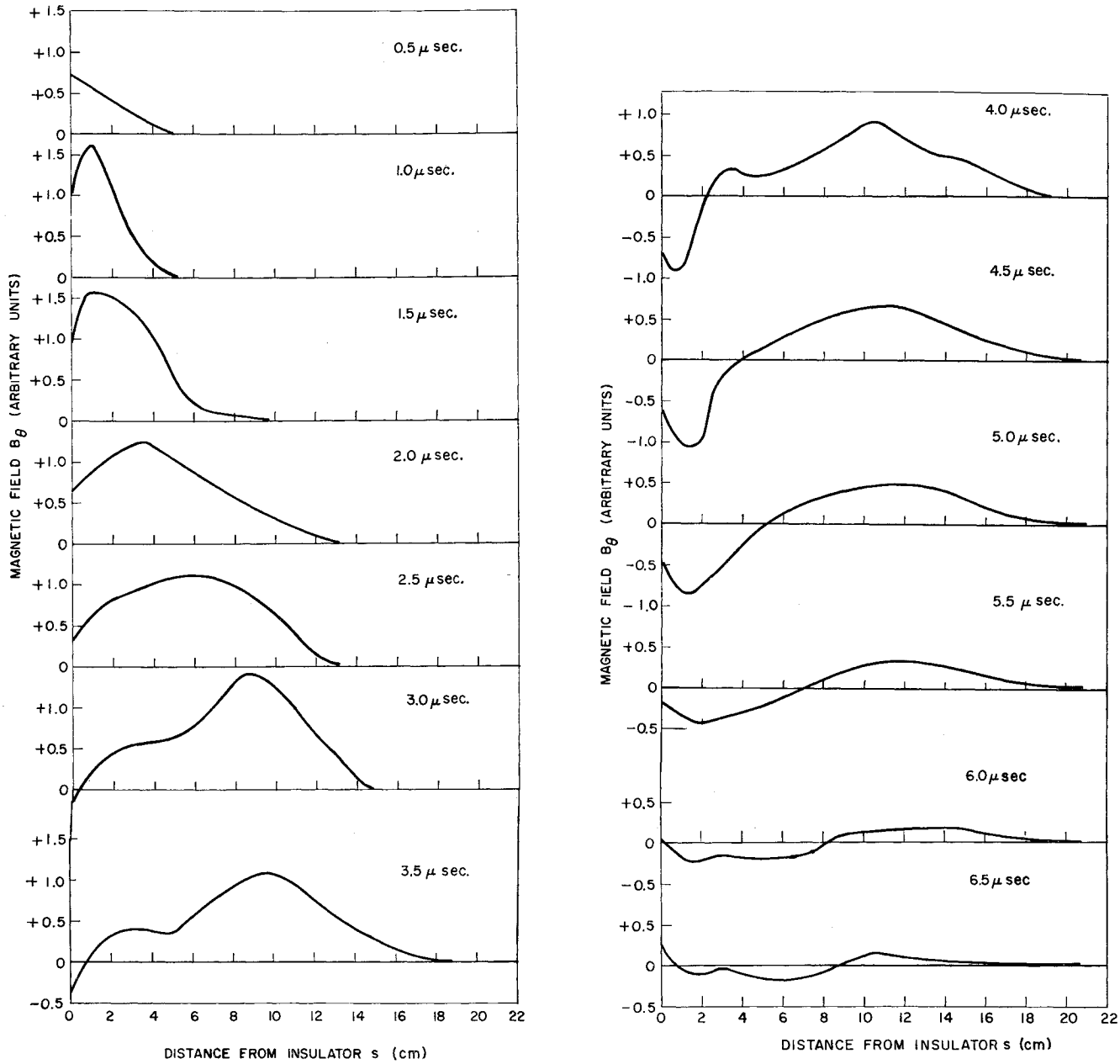

Fig. 5 Magnetic field vs distance from insulator.

signal at each position indicated that the discharge was essentially symmetric above capacitor potentials of 2.5 kv. These results indicated that the discharge was a sheet that was nearly uniform in the azimuthal direction. Consequently, any "spoke" asymmetries that exist would be small perturbations of the main discharge and would not be expected to have a significant influence on the characteristics of the accelerator.

From the oscilloscope traces, the magnetic field can be plotted as a function of s at various times, where s is the distance from the insulator measured along the centerline of the interelectrode gap. The data were taken at eight positions along the electrodes. (This was accomplished by constructing probes so that the magnetic field could be measured at two s points from each of the hole locations shown in Fig. 2.) Probes were also placed beyond the exit (s = 17.0 cm) to measure the trapped magnetic field in the plasma exhaust. The value of the magnetic field at the insulator (s = 0) was calculated from the total current, as measured by the Rogowski coil, from the relation

$$B_\theta = \mu_0 I/2\pi r_0 \qquad (1)$$

where I is the total discharge current, r_0 is the inside radius of the insulator measured from the symmetry axis of the electrodes, and $\mu_0 = 4\pi \times 10^{-7}$ h/m.

The results are shown in Fig. 5. The propagation of the magnetic field down the electrodes is apparent. If the thickness of the current sheet is taken as the distance over which the magnetic field rises from zero to its maximum value, the minimum thickness is about 4 cm at 1.0 μsec. The large thickness is a consequence of a relatively low electrical conductivity. Therefore, the assumption that a current sheet has zero thickness and infinite conductivity, although applicable to many thermonuclear plasmas, is questionable when applied to plasma accelerators.

The leading edge of the current sheet advances faster than the peak, and thus the current sheet becomes thicker as it moves toward the exit. This same general behavior was observed by Burkhardt and Lovberg[6] in a coaxial plasma gun. The thickening of the current sheet may be due to the decrease in magnetic pressure during the second quarter-cycle of discharge current. During this period, the plasma pressure may be greater than the magnetic pressure, allowing the trailing edge of the current sheet to expand in the reverse

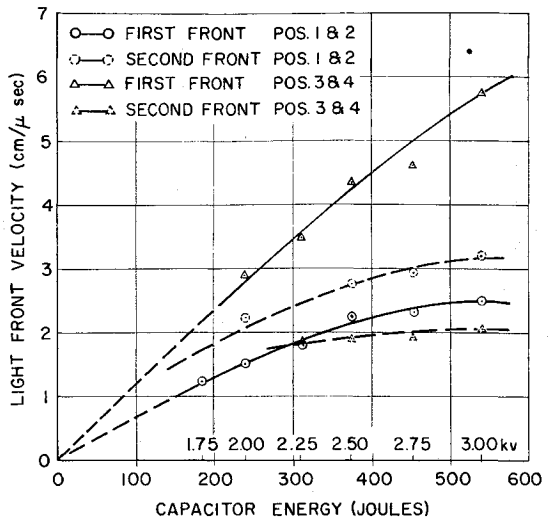

Fig. 6 Velocity of first and second light fronts vs capacitor energy.

direction and consequently lose velocity while leading edge tends to maintain its velocity.

Since the second half-cycle of current begins at about 3 μsec, B_θ at the insulator becomes negative at that time. The first probe (position 1 at $s = 1.1$ cm) does not record a negative magnetic field until about 4.0 μsec, indicating that the second current sheet remains near the insulator up to this time. For later times, the second current sheet is seen to have a slightly smaller thickness than the first current sheet, but it does not propagate down the electrodes.

It is of interest to compare the behavior of the second current sheet with results of photocell measurements of the light front velocities. The first, second, and third light fronts were recorded at positions 1–4 with RCA 1P42 photocells. The third light front was of very small amplitude, and it appeared to be rather diffuse. Consequently, its velocity could not be determined with any degree of accuracy.

Figure 6 shows the velocities of the first and second light fronts as a function of the capacitor energy. It is seen that, as expected, the velocity of the first light front between positions 3 and 4 is greater than the velocity between 1 and 2. However, the velocity of the second light front decreases as it travels along the electrodes. It is noted that, between positions 1 and 2, the velocity of the second front is initially higher than that of the first front, possibly because the second discharge takes place in a gas that is already partially ionized.

The deceleration of the second front agrees well with the magnetic probe data. (Note that the second light front reaches position 3, $s = 11.6$ cm, between 6 and 7 μsec and position 4, $s = 15.1$ cm, between 7 and 8 μsec.) The magnetic field due to the second half-cycle does not propagate beyond position 2($s = 6.2$ cm). Concurrently, there is still a residual magnetic field due to the first half-cycle beyond this point. Consequently, instead of being driven by a magnetic field, as in the case for the plasma associated with the first light front, the plasma associated with the second front propagates through a magnetic field. This, together with the viscous drag that exists, accounts for its deceleration. Therefore, it can be concluded that the accelerator produces only one pinch that accelerates the plasma associated with the first light front and that is due to the first half-cycle of current.

Current Sheet Orientation

In order to determine if the current sheet remains perpendicular to the electrodes while its motion changes from the radial to the axial direction, the time of arrival of the magnetic field was measured transverse to the plasma flow for both positive and negative polarity of the inner electrode. (The accelerator is normally operated with the center electrode positive.) The measurements were made by mounting three magnetic probes in a line perpendicular to the electrodes at each position. Results showed that for both polarities the current sheet position at the inner electrode and the position at the outer electrode differed by less than about 1 cm along the entire electrode length, so that the current sheet remained roughly perpendicular to the electrodes at all times.

It has been suggested by Gloersen[7] that in a pinch accelerator "the initial radial motion of the plasma is converted to axial motion solely by collisions with the curved electrode surfaces, since no appropriately curved magnetic field lines are present for this purpose." However, the small cant and perpendicular orientation of the current sheet indicates that the magnetic force is acting on the plasma approximately in the direction of plasma motion, i.e., in the direction of s, through the entire length of the electrodes. Gloersen's statement implies that the plasma being accelerated must collide with the inner electrode before it changes direction. However, since the plasma being accelerated is in the current sheet and subject to magnetic forces, it can change direction without collisions with the inner electrode. Undoubtedly, some of the plasma does collide with the walls, and these collisions do affect the orientation of the current sheet, but the fraction of the plasma making these collisions should be small.

There are two physical reasons why the motion of the current sheet changes from the radial direction. The first is that, at least ahead of the current sheet, the electric field applied to the electrodes from the capacitors will be perpendicular to the electrodes. The current will tend to follow the direction of the electric field. The second reason is that, once the current sheet has begun to turn, the magnetic pressure, which varies as r^{-2}, is greater at the inner electrode and thus will tend to turn the current sheet more. The motion of plasmas in curved electrodes was investigated analytically by Guman,[8] who showed that certain electrode geometries exist in which a slug-type axisymmetric current sheet will orient itself relative to a curved electrode in such a way that the component of the magnetic force normal to the wall will just balance the local centrifugal force. In such geometries, the current sheet will not be subjected to a force by the wall, and, consequently, no direct interaction between the sheet and the wall will occur.

Current Distribution

The current distribution, assumed to be axially symmetric, was calculated from the B_θ vs s curves. The value of B_θ at position s is given by

$$B_\theta = \frac{\mu_0}{2\pi r_s}\int_s^{s_1} j(s)ds \qquad (2)$$

where r_s is the distance from s in meters to the symmetry axis, and the integral is the current in amperes between s and the leading edge of the current distribution which is at a position s_1. The current per unit length $j(s)$ is defined by $dI = j(s)ds$, where dI is the current crossing the element of area generated by rotating ds about the axis of symmetry of the electrodes. Differentiating Eq. (2) with respect to s yields

$$j(s) = -(2\pi/\mu_0)(\partial/\partial s)(r_s B_\theta) \qquad (3)$$

The current density $J(s)$ is related to $j(s)$ by $J(s) = j(s)/2\pi r_s$, where it is assumed that $J(s)$ is normal to s.

Various schemes were used for computing $j(s)$ from the measured values of B_θ. Hand computation appeared to be the most reliable method. The most difficult and time-consuming part of the hand computation, as well as the operation in which the most uncertainty was introduced, was the determination of the derivative of the $r_s B_\theta$ curve which was

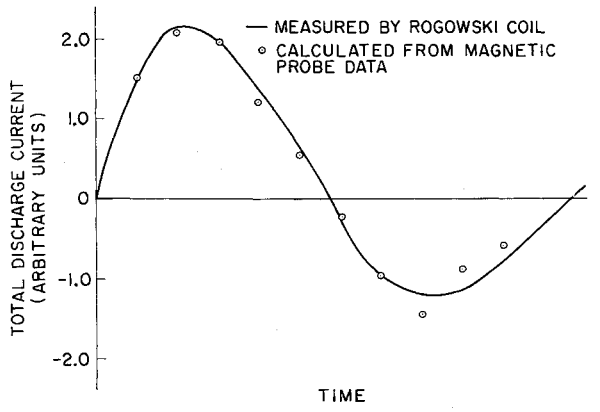

Fig. 7 Comparison of total discharge current measured by Rogowski coil with values calculated from magnetic probe data.

obtained by fitting slopes by eye to the curve. Consequently, digital computer programs were used to simplify data processing. The most successful computer method used parabolic interpolation between data points to obtain the derivative. However, this procedure introduced a few doubtful peaks into the computed results. Another scheme used a higher-order polynomial least-squares fit to the data points.

As a check on the accuracy of the $j(s)$ distribution, the integral

$$I = \int_0^{s_1} j(s)ds \tag{4}$$

was compared with the discharge current measured with a Rogowski coil. Both of these digital computer methods gave fair agreement with the current values measured by the Rogowski coil, but the agreement of the hand-computed results was better. The comparison of the hand-computed results and the Rogowski coil measurement is shown in Fig. 7, and the agreement is seen to be very good up to the peak of the second half-cycle.

Plots of $J(s)$ vs s at 0.5-μsec intervals are shown in Fig. 8. It is seen that the current sheet is concentrated near $s = 0$ at the beginning of the discharge. During this interval, current densities in excess of 10^7 amp/m^2 occur. After 1 μsec, the current sheet moves down the electrodes, becoming progressively more diffuse. Similar results were obtained using nine 40-μf capacitors charged to 1.44 kv which were substituted for the capacitor bank used in the study.

The reversal of current direction at small values of s occurring during the first half-cycle of the total discharge current can be seen in Fig. 8. This reversal of current is due to loop currents that have been observed in other plasma accelerators using capacitive discharges.[9] During the second quarter-cycle, the total discharge current is decreasing, which tends to decrease the magnetic flux in the interelectrode space. Because this space is filled with plasma, eddy currents that take the form of closed loops are induced to oppose the change in flux. Near the leading edge of the current distribution, the loop currents are in the same direction as the current from the capacitor bank, whereas at the rear of the distribution, the loop currents are in the opposite direction. It should be noted, however, that this explanation does not account for loop currents during the first quarter-cycle (before 1.5 μsec).

An interesting phenomenon was observed in the current distributions for times greater than 3.0 μsec. It is noted in Fig. 8 that, at 3.0 μsec, two positive peaks separated by a negative region appear. Apparently, the direction of current density at any instant may show regions in which there are local reversals in current direction. Because of the decreasing values of B_θ and the broadening of the B_θ distribution, the sensitivity of the measurements becomes insufficient to resolve accurately the local structure at substantially later times.

$J \times B$ Force Distribution and Impulse

The magnetic ($J \times B$) force distribution acting on the plasma can be calculated from the magnetic field and current distributions and is plotted in Fig. 9 at 0.5-μsec intervals. A force distribution function $f(s)$ is defined by the expression $dF = f(s)ds$, where dF is the component along s of the magnetic force on an element of plasma contained between two planes located at s and $s + ds$, the planes being taken normal to s. The distribution $f(s)$ is given by

$$f(s) = j(s)B_\theta(s)h(s) \tag{5}$$

where h is the interelectrode gap spacing. The total force $F(t)$ on the plasma at time t is the integral of $f(s)$ over the length of the electrodes. More accurately, it is the integral over the current distribution, some of which extends outside the nozzle at later times. However, the contribution of this external portion is small.

The impulse given to the plasma by the $J \times B$ force is the integral of $F(t)$ over the time of the discharge. Conse-

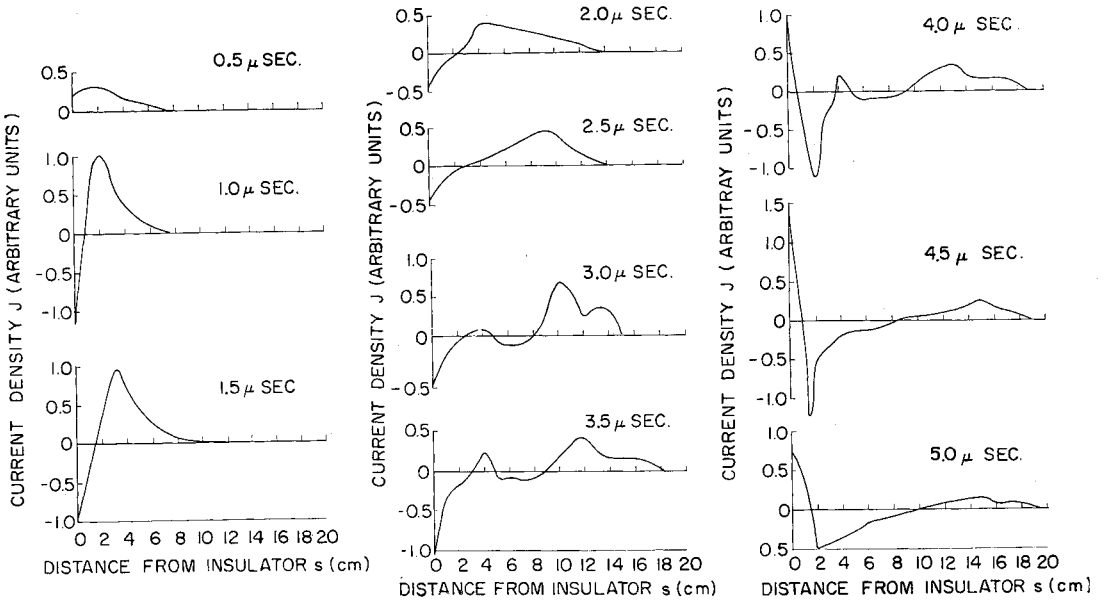

Fig. 8 Current density vs distance from insulator.

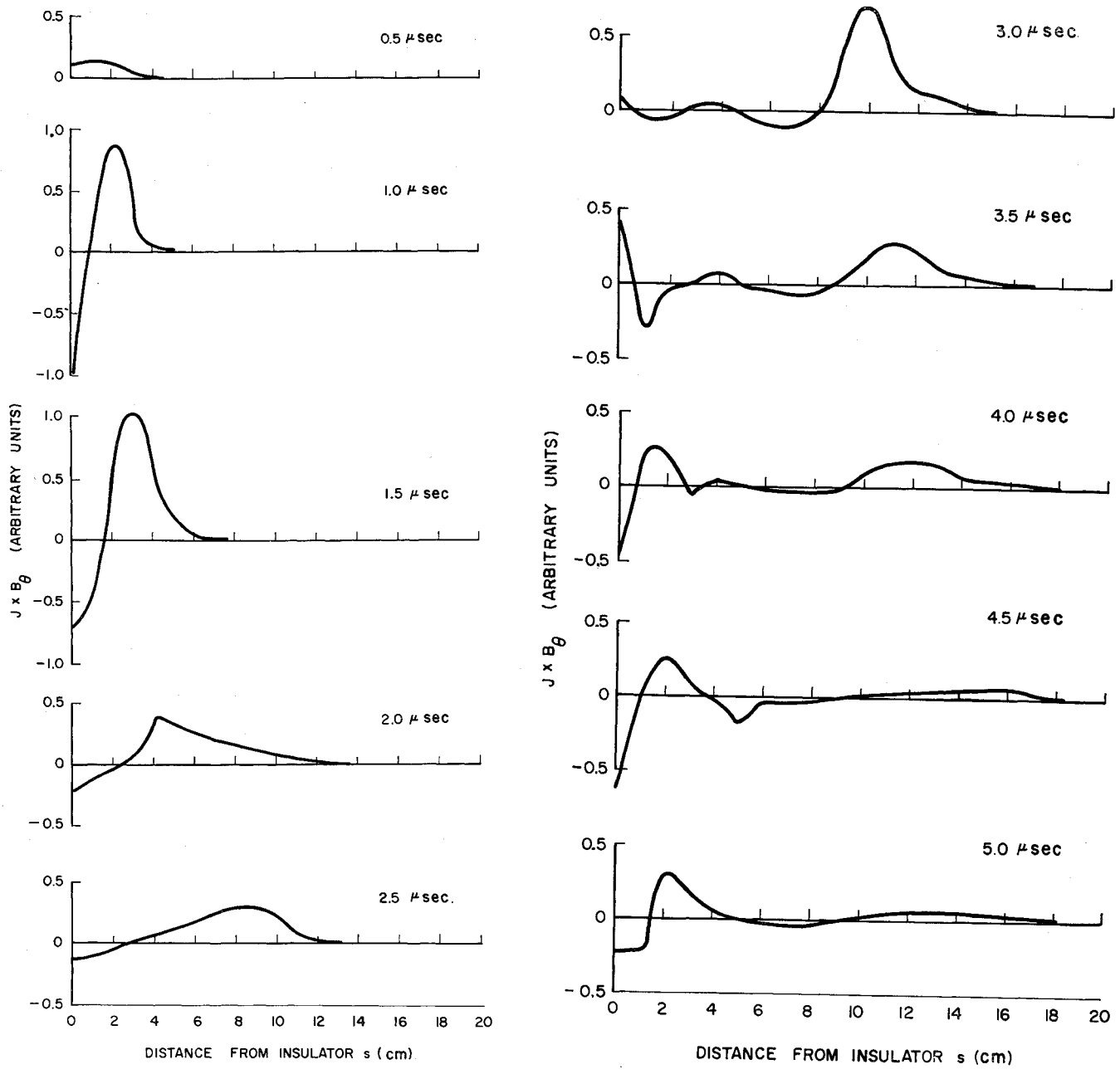

Fig. 9 $J \times B$ force vs distance from insulator.

quently, although the $J \times B$ distribution depends on the processes by which momentum is transferred to the plasma, it is not necessary to consider these processes in order to compute the impulse.

When comparing the impulse imparted to the plasma by $F(t)$ with the impulse of the accelerator as measured on a thrust stand, some uncertainty is introduced by the negative portions of the $f(s)$ curves which may be quite large at small values of s (see Fig. 9). These forces, which are directed away from the exit, will accelerate plasma toward the insulator. This plasma flow will most likely move toward the insulator and be stagnated there. Then, by re-expanding, it could contribute some positive impulse to the accelerator. However, such a conversion from $J \times B$ to thermal impulse would be relatively inefficient. Therefore, the negative portions of $f(s)$ were neglected, and only the positive leading portions were used to compute $F(t)$. For example, from the $J \times B$ curve for 3.0 μsec in Fig. 9, it can be seen that $f(s)$ is positive for s greater than approximately 8 cm. Only this positive portion of the $f(s)$ distribution was used to calculate $F(t)$ at 3.0 μsec. The values of $f(s)$ for s less than 8 cm, where $f(s)$ has both negative and positive regions, were neglected. This method of calculating $F(t)$ neglects the possibility that some of the mass acted upon by a positive force could subsequently be acted upon by a negative force. Consequently, some of the impulse would be lost. Unfortunately, it is exceedingly difficult to estimate what fraction of the mass would be affected. Certainly, the negative force near the insulator at later times does not affect the plasma being accelerated by the first half-cycle and thus can safely be neglected.

A plot of $F(t)$ vs t is shown in Fig. 10. The impulse calculated from this plot is approximately 80% of the impulse produced by the accelerator as measured by a thrust stand. If both the positive and negative portions of the $f(s)$ curve are used to compute $F(t)$, the calculated impulse is about 50% of the measured value. However, as previously mentioned, this value is certainly low.

These results are consistent with the previously mentioned probe measurements, which showed that the magnetic force is essentially in the direction of plasma motion, indicating that it could be the principal force acting on the plasma.

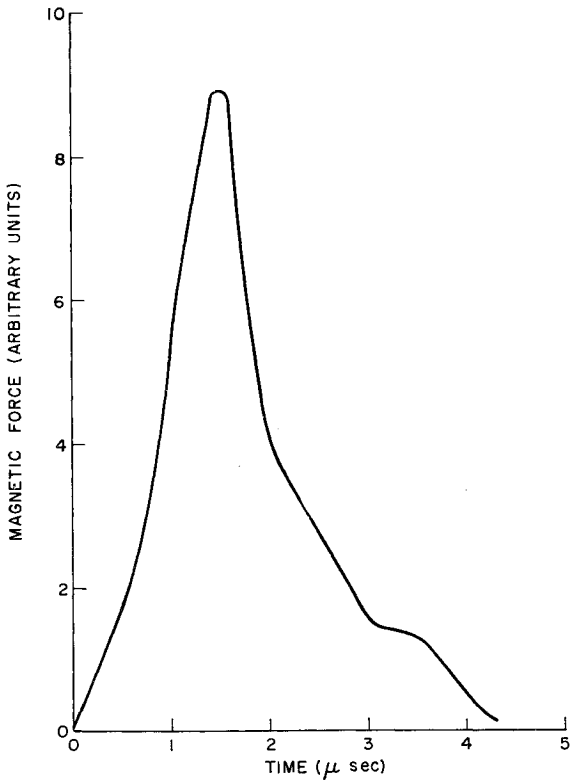

Fig. 10 Magnetic force on plasma vs time.

The agreement between computed and measured impulse indicates that the impulse comes primarily from the $J \times B$ force and that other contributions to the impulse, such as the subsequent hot-gas flow, are small. It also indicates that various drag losses that could prevent the full $J \times B$ impulse from appearing as accelerator impulse are small.

Capacitor Power and Energy Output

From simultaneous capacitor voltage and total discharge current measurements, as illustrated in Fig. 3, the power output of the capacitors was calculated as a function of time and is shown in Fig. 11. The negative portions of the curve represent the power return to the capacitors from the inductive elements of the circuit. It is seen that after 2.4 μsec the power output of the capacitors is essentially balanced by the power returned. This is shown more clearly by the curve representing the total energy transferred from the capacitors to the accelerator as a function of time which was obtained by integrating the power curve. It is of interest to note that the shape of the power input curve is nearly identical to that obtained by Gooding, Hayworth, and Lovberg[10] using a coaxial plasma gun. This similarity is rather surprising in view of the difference in the geometry and electrical parameters of the two accelerators.

The power and energy output are in qualitative agreement with the velocity and acceleration of the current sheet as determined by the magnetic probe and photocell data. It was found that the current sheet accelerates up to about 2 μsec and subsequently travels at constant velocity until it reaches the exit. The current sheet appears to stop accelerating because the net power input to the accelerator is approaching zero. The probable reason that the magnetic field due to the second half-cycle does not propagate down the electrodes is that there is no net power input during the second half-cycle.

McIlroy and Siegel[11] have shown in a dimensionless snowplow analysis that for maximum efficiency the plasma should reach the accelerator exit when the voltage reaches zero. The obvious physical reason for this result is that, after the

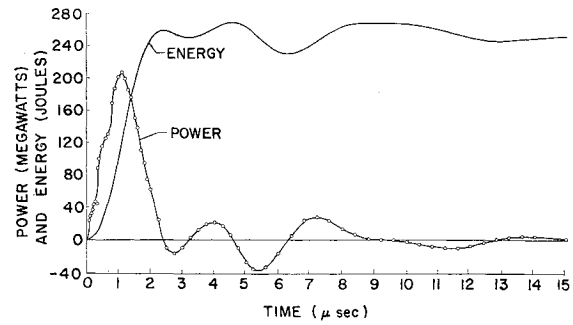

Fig. 11 Power and energy output of capacitor bank vs time.

voltage goes through zero, the power input to the accelerator becomes negative, as illustrated by Fig. 11. It can be concluded that the performance of this accelerator could be improved by redesigning the electrodes so that the current sheet reached the exit at 2.4 μsec. An average value of the sheet position would have to be used, however, since the thickness of the current sheet is relatively large at this time.

It is noted that about 255 joules are transferred to the accelerator, which is less than half of the 540 joules stored in the capacitor bank at 3 kv. The remaining energy must be dissipated in the capacitors as an I^2R loss. The capacitors are, therefore, not well suited to efficient operation with this type of accelerator.

The efficiency of a plasma accelerator obviously also depends on the fraction of the energy leaving the capacitors which is converted to plasma kinetic energy. The efficiency of this accelerator is low because there is a poor "match" between the various electrical, geometric, and magnetogasdynamic parameters. This low efficiency can be advantageous in diagnostic studies by making the discharge current less sensitive to changes in some of the parameters. Thus, the effects of varying these quantities can be studied while holding the discharge current relatively constant.

The dependence of the discharge current on the magnetogasdynamic characteristics can be seen in Fig. 12, which shows the discharge current for a type of accelerator similar to the one discussed in this paper, except that the parameters are better matched. Figure 12a shows the trace that results from discharging the capacitor bank by connecting a short circuit across the exit end of the electrodes. The trace is seen to be a typical damped l.c. discharge. Figure 12b shows the discharge current occurring during actual plasma acceleration. It is seen that the current is highly damped, the second quarter-cycle being almost negligible. Therefore, a greater percentage of the input energy should be transferred to the plasma.

Effect of Propellant

The plasma exhaust velocity of the accelerator was determined using four gases as the propellant: hydrogen, helium, nitrogen, and freon. The exhaust velocity was determined as a function of the energy stored in the capacitors from time of arrival data obtained at positions 5 and 6 by means of photocells (see Fig. 2). The gas supply pressure was set just slightly higher than the minimum value that would initiate the discharge. The approximate supply pressures were as follows: hydrogen, 40 mm Hg; helium, 60 mm Hg; nitrogen, 40 mm Hg; and freon, 10 mm Hg.

The results are presented in Fig. 13. It is seen that, although the plasma velocity decreases with increasing molecular weight of the gas, the velocities for the gases heavier than hydrogen do not differ by much. Essentially the same results were obtained with a similar accelerator that had a different set of electrodes, capacitor bank, and type of propellant valve.

In interpreting these results, it must be remembered that, since the gas is admitted by a valve and because the gas supply pressures differed, the density of the gas in the interelectrode space at the initiation of the discharge is different for each gas, even though the valve is operated in exactly the same manner. Consequently, the effect of the gas itself cannot be determined from these data. It does appear, however, that, for a pinch accelerator in which the discharge is initiated by the propellant admitted from a valve, the plasma velocity does not differ much for any gas except hydrogen.

These results are similar to those obtained by Michels and Ramins[12] and by Keck.[13] Michels and Ramins, using hydrogen, nitrogen, and argon in a coaxial plasma gun, found that the magnetic front velocity decreased only slightly with increasing molecular weight when the mass of each gas admitted was approximately the same. However, since they also used a valve, definite conclusions regarding the effect of molecular weight could not be drawn. Keck, using hydrogen, helium, air, and argon in a magnetic annular (coaxial) shock tube, found that the current sheet velocity, as measured with ultraviolet detectors, was nearly independent of molecular weight. The observed velocity in hydrogen was only about 20% higher than in argon. Since the shock tube was filled to the same specified gas pressure in each case, there was no uncertainty in the gas density at the time of initiation of the discharge.

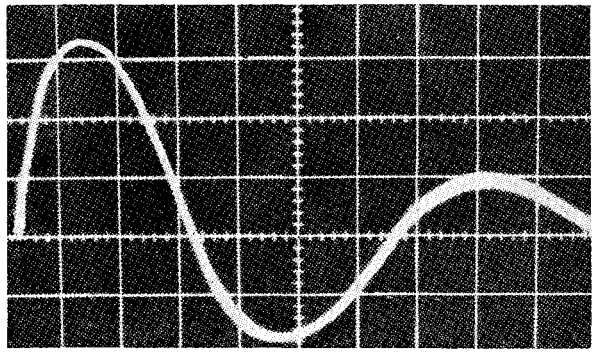

a) Short-circuited electrodes

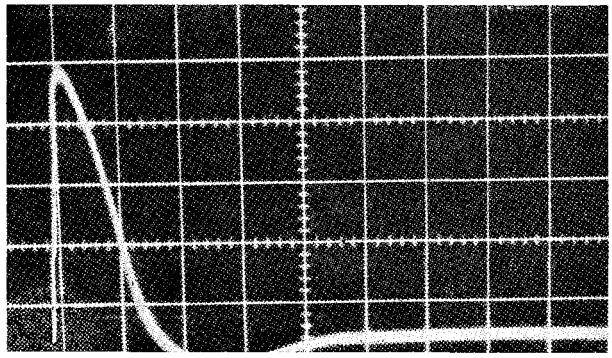

b) Discharge

Fig. 12 Total current traces of "matched" accelerator. Sweep speed of 12a is 2.5 times sweep speed of 12b.

The preceding results indicate that inertia of the gas is not the principal limitation on the current sheet velocity. Keck suggests that velocity is limited by the material ablated from the insulator. Under certain conditions, electrode ablation might also limit velocity.

It should be noted that in Ref. 1 the plasma velocity appeared to vary linearly with the energy stored in the capacitors. In Fig. 13, it is seen that the curve for hydrogen deviates from a straight line at about 250 joules, and the curves for the heavier gases deviate at somewhat higher energies. However, the deviation for the heavier gases is quite small. The discrepancy between Fig. 13 and the data reported in Ref. 1 can be attributed to the greater scatter of the previous data.

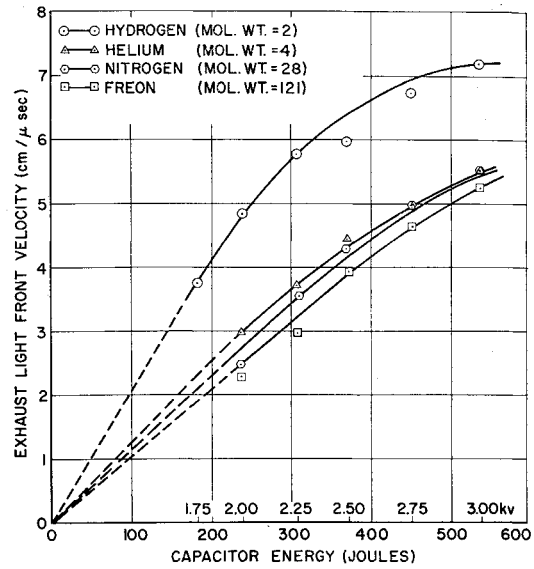

Fig. 13 Light front velocity of exhaust plasma vs capacitor energy for various propellants.

Electron Density

Indications of the electron density in the accelerator exhaust were obtained from microwave interferometer[14] and from double electric probe measurements. It was estimated that the maximum electron density is over 10^{14} electrons/cm^3 and may be as high as 5×10^{15} electrons/cm^3. These estimates are higher than previous estimates of the exhaust electron density.[1] Exact measurements could not be made, since microwave equipment is not available which will measure densities over 10^{14} electrons/cm^3, and probe theory to date is valid only for lower densities.

Conclusions

The important conclusions resulting from this study can be summarized as follows:

1) The current sheet propagates down the electrodes, becoming more diffuse with time. Its minimum thickness is about 4 cm.

2) Only the current sheet due to the first half-cycle of current propagates down the electrodes. Therefore, only one pinch is produced.

3) The motion of the current sheet turns from the radial to the axial direction. The magnetic force on the plasma is approximately in the direction of plasma motion.

4) There are regions behind the current sheet where the the direction of current shows local reversals.

5) The magnetic impulse represents the largest part of the impulse produced by the accelerator.

6) All of the net energy transferred from the capacitors to the accelerator is transferred during the first 2.4 μsec.

7) The plasma exhaust velocity decreases with increasing molecular weight of the propellant, but the variation with molecular weight is small.

References

[1] Aronowitz, L. and Duclos, D. P., "Characteristics of the pinch discharge in a pulsed plasma accelerator," *Electric Propulsion Development*, edited by E. Stuhlinger (Academic Press, New York, 1963), Vol. 9, pp. 513–530.

[2] Glasstone, S. and Lovberg, R. H., *Controlled Thermonuclear Reactions* (D. Van Nostrand Co. Inc., Princeton, N. J., 1960), p. 230.

[3] Sergre, S. E. and Allen, T. E., "Magnetic probes of high frequency response," J. Sci. Instr. **37**, 369–371 (1960).
[4] Gooding, T. J., Hayworth, B. R., and Lovberg, R. H., "Instabilities in a coaxial plasma gun," AIAA J. **1**, 1289–1292 (1963).
[5] Jahn, R. G. and von Jaskowsky, W., "Structure of a large-radius pinch discharge," AIAA J. **1**, 1809–1814 (1963).
[6] Burkhardt, L. C. and Lovberg, R. H., "Current sheet in a coaxial plasma gun," Phys. Fluids **5**, 341–347 (1962).
[7] Gloersen, P., "Pulsed plasma accelerators," ARS Preprint 2129-61 (October 1961).
[8] Guman, W. J., "Dynamic behavior of nonsteady axisymmetric magnetically driven slug-type plasma sheets," Ph.D. Thesis, Dept. Aeronaut. Eng., Rensselaer Polytechnic Inst. (1963).
[9] Hart, P. J., "Plasma acceleration with coaxial electrodes," Phys. Fluids **5**, 38–47 (1962).
[10] Gooding, T. J., Hayworth, B. R., and Lovberg, R. H., "Physical processes in a coaxial plasma gun," AIAA Preprint 63004 (March 1963).
[11] McIlroy, W. and Siegel, B., "Analysis of factors influencing plasma engine performance," Am. Soc. Mech. Engrs. Hydraulics, Gas Turbine, Aviation and Space Meeting, Los Angeles (March 3–7, 1963).
[12] Michels, C. J. and Ramins, P., "Performance of coaxial plasma gun with various propellants," International Symposium on Plasma Coaxial Guns, Cleveland (September 6–7, 1962).
[13] Keck, J., "Current speed in a magnetic annular shock tube," Avco-Everett Research Lab., Res. Rept. 152 (May 1963).
[14] Steinberg, A. and Levy, G., "Determination of pinch plasma engine exhaust profiles by microwave interferometry techniques," Inst. Electrical Engrs. International Convention, New York (March 25–28, 1963).

NOVEMBER 1963 AIAA JOURNAL VOL. 1, NO. 11

Conductivity Probe Measurements in Flames

R. A. Olson* and E. C. Lary†
United Aircraft Corporation, East Hartford, Connecticut

An electrodeless probe has been developed to measure the electrical conductivity of high-temperature gases or flames. The weak interaction of an rf field with a plasma is employed to measure the conductivity in the immediate vicinity of the probe. The probe overcomes the principal difficulties associated with techniques employing electrodes or microwaves and is generally applicable to subsonic flows. Values of conductivity in the range of 0.04 to 0.27 mho/m have been detected with the probe in traversing an alkali-seeded hydrogen-oxygen flame. The same probe has shown a linear response to the conductivity of electrolytic solutions of up to 40 mho/m.

Introduction

SEVERAL techniques have been advanced for measuring the electrical conductivity of flames. The most common techniques have difficulties associated with the use of electrodes, including the effects of boundary layers, electrical sheaths, contact potentials, and thermionic emission.[1] These difficulties have been overcome in several investigations by the use of an electrodeless interaction with the flame. Williams[2] employs a resonant coil surrounding the flame to obtain a relative measurement of dissipation in the flame. The primary difficulty here is that only an average measurement over a large region of the flame can be obtained and that absolute values of conductivity were not obtained. Microwave techniques used by still other investigators (e.g., Ref. 3), though having many advantages, involve an average of the interaction over the entire path length through the flame.

A conductivity measurement probe has been developed in order to overcome difficulties in the measurement of plasma conductivity in MHD devices.[4] The probe detects the conductivity in its immediate vicinity by dissipating a very small amount of rf power in the plasma. The weak interaction with the plasma is detected by observing the resistive loading of a sensitive rf oscillator-detector. Ring currents are induced in the plasma, about the insulated probe, so that the difficulties associated with electrodes are eliminated. Moreover, the measuring frequency of about 20 Mc/sec is well below the electron collision frequency of the flame, insuring that the d.c. electrical conductivity is measured by the rf probe.

The electrodeless probe technique has been applied to the measurement of the conductivity of electrolytes, semiconductors, low-density plasmas (including rf discharge plasmas), and the high-temperature ionized-gas flow of an MHD generator. More recently, the technique has been employed in the measurement of flame conductivity. This application required a miniaturization of the probe, as well as improved instrumentation, in order to detect and resolve very small values of conductivity. At the same time, a simplification of the probe design (with the elimination of the need for cooling) was achieved by traversing the probe very quickly through the flame. The outer shell of the probe is an insulator, thereby eliminating spurious thermal effects during the period of probing.

Conductivity Measurement Probe

The conductivity probe is basically a single-layer, tightly wound helical coil impressed with rf currents by an external circuit. The coil acts as the primary of an rf transformer in which the plasma is a short-circuited secondary that dissipates a small amount of power. The coil produces an

Presented at the ARS Ions in Flames and Rocket Exhausts Conference, Palm Springs, Calif., October 10–12, 1962; revision received August 23, 1963. The authors wish to express their gratitude to several colleagues for their helpful efforts; especially to A. Witherell for the careful development and construction of the conductivity probes and experimental apparatus, to A. Kozubal for the design of the rf instrumentation, and to W. Price for the microwave measurements. The authors also wish to thank Irvin Glassman of Princeton University for suggesting this application of the conductivity probe.

* Research Scientist, Magnetohydrodynamics, Research Laboratories.
† Principal Scientist, Magnetohydrodynamics, Research Laboratories.